Journal of Colloid and Interface Science 663 (2024) 869–879

Contents lists available at ScienceDirect

Journal of Colloid And Interface Science

journal homepage: www.elsevier.com/locate/jcis

Microporous electrospun nonwovens combined with green solvents for the selective peel-off of thin coatings from painting surfaces

Francesca Ramacciotti [a], Giorgia Sciutto [a], Laure Cazals [b], Denise Biagini [c], Serena Reale [c], Ilaria Degano [c], Maria Letizia Focarete [a,d,e], Rocco Mazzeo [a], Mathieu Thoury [f], Loïc Bertrand [b], Chiara Gualandi [a,d,g,*], Silvia Prati [a,*]

[a] Department of Chemistry "Giacomo Ciamician", University of Bologna, Via Selmi 2, 40126 Bologna, Italy
[b] Université Paris-Saclay, ENS Paris-Saclay, CNRS, Photophysique et Photochimie Supramoléculaires et Macromoléculaires, 91190 Gif-sur-Yvette, France
[c] Department of Chemistry and Industrial Chemistry, University of Pisa, Via Moruzzi 13, 56124 Pisa, Italy
[d] INSTM UdR of Bologna, University of Bologna, Via Selmi 2, 40126 Bologna, Italy
[e] Health Sciences & Technologies (HST) CIRI, University of Bologna, Via Tolara di Sopra 41/E, 40064 Ozzano Emilia Bologna, Italy
[f] Université Paris-Saclay, CNRS, Ministère de la Culture, UVSQ, MNHN, Institut Photonique d'Analyse Non-destructive Européen des Matériaux Anciens, Saint-Aubin, 91192, France
[g] Interdepartmental Center for Industrial Research on Advanced Applications in Mechanical Engineering and Materials Technology, CIRI-MAM, University of Bologna, Viale Risorgimento, 2, 40136 Bologna, Italy

GRAPHICAL ABSTRACT

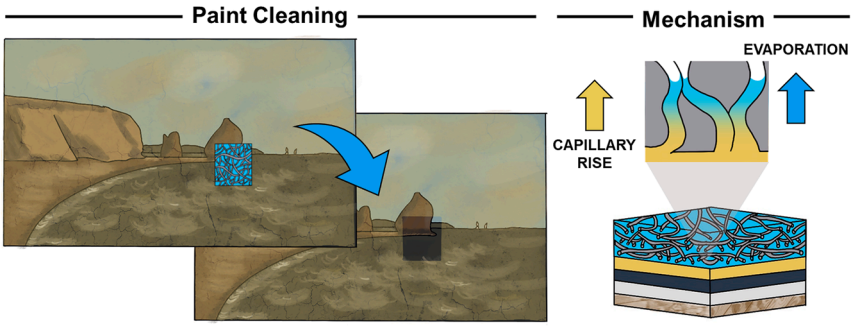

ARTICLE INFO

Keywords:
Electrospinning
Dimethyl carbonate
Cleaning of paintings
Green solvent
Capillary rise

ABSTRACT

Over the last few decades, significant research efforts have been devoted to developing new cleaning systems aimed at preserving cultural heritage. One of the main objectives is to selectively remove aged or undesirable coatings from painted surfaces while preventing the cleaning solvent from permeating and engaging with the pictorial layers. In this work, we propose the use of electrospun polyamide 6,6 nonwovens in conjunction with a green solvent (dimethyl carbonate). By adjusting the electrospinning parameters, we produced three distinct nonwovens with varying average fiber diameters, ranging from 0.4 μm to 2 μm. These samples were characterized and tested for their efficacy in removing dammar varnish from painted surfaces. In particular, the cleaning process was monitored using macroscale PL (photoluminescence) imaging in real-time, while post-application examination of the mats was performed through scanning electron microscopy. The solvent

* Corresponding authors.
E-mail addresses: c.gualandi@unibo.it (C. Gualandi), s.prati@unibo.it (S. Prati).

https://doi.org/10.1016/j.jcis.2024.03.006
Received 19 December 2023; Received in revised form 20 February 2024; Accepted 1 March 2024
Available online 2 March 2024

evaporation rate from the different nonwovens was evaluated using gravimetric analysis and Proton Transfer Reaction- Time-of-Flight. It was observed that the application of the nonwovens with small or intermediate pore sizes for the removal of the terpenic varnish resulted in the swollen resin being absorbed into the mats, showcasing a peel-off effect. Thus, this protocol eliminates the need for further potentially detrimental removal procedures involving cotton swabs. The experimental data suggests that the peel-off effect relates to the microporosity of the mats, which enhances the capillary rise of the swollen varnish. Furthermore, the application of these systems to historical paintings underwent preliminary validation using a real painting from the 20th century.

1. Introduction

Current research in restoration is primarily focused on the development of innovative chemical cleaning systems, to be employed especially in a situation when the solvent used for cleaning may compromise the substrate's chemical and/or physical integrity [1]. Historically, in Western countries, natural resins (*e.g.,* dammar, sandarac, and mastic) were employed to prepare varnishes, serving both as protective coatings and enhancers of the visual aesthetics of paintings [2,3]. Over time, environmental factors like light, temperature, humidity, and contaminants induce the degradation of the varnish layers, leading to alterations in their optical, physical, and chemical properties [4]. The removal of aged varnishes traditionally involves using solvents as cleaning agents, applied to the painting through methods like cotton swabs or thickened pastes. However, these approaches suffer from poor confinement of the solvent, whose release is, therefore, scarcely controlled [5]. Consequently, the interaction between the organic solvent and the paint layer may compromise the integrity of the latter, triggering embrittlement and/or swelling of the paint, redistribution of paint-soluble components, and saponification [6,7]. In addition, traditional organic solvents are characterized by high volatility and toxicity, posing risks to both operators and the environment [8,9]. Hence, there is a growing need for alternative cleaning systems that mitigate these drawbacks and provide more precise control over the cleaning process.

Chemical and physical gels have become a common alternative to cotton swabs thanks to their solvent retention ability, although the need for mechanical removal of residues from the swelled varnish and/or gel persists [10,11]. Additionally, there has been a recent emphasis on cleaning methods that align with environmental sustainability principles. In this regard, green organogels derived from the gelation of the biobased polymer poly(3-hydroxybutyrate) (PHB) with green solvents have been proposed in recent literature [1,7,12,13]. As a further advancement, aiming to minimize surface residues and enhance control over solvent release, we have introduced novel sandwich-like composites combining PHB-based green organogel with electrospun nonwovens. This integrated cleaning system has demonstrated a reduction in gel residues, as well as improvements in gel handling and cleaning performance, also in terms of controlled solvent release [14].

Electrospinning is a technique employed to produce ultrathin fibers using electrostatic forces to uniaxially stretch a viscoelastic jet derived from a polymer solution or melt [15]. This versatile technique enables the fabrication of a wide variety of nanostructured materials (such as fibers, membranes, bundles) with controlled diameter, size, morphology, and composition [16,17]. Its applications span various fields, encompassing tissue engineering, catalysis, enzyme supports, sensors, and energy storage devices [18,19]. Furthermore, electrospun nanofibers are being investigated for sorbent applications, including microextraction and air and wastewater filtration, owing to their ability to incorporate nanoparticles by exploiting high porosity and surface area [20–24]. Notably, electrospinning stands out from other spinning techniques by its ability to fabricate fibers with diameters smaller than a micrometer and pore sizes of a few microns.

In this work, we propose a novel and straightforward cleaning system designed for the selective removal of coatings from paintings. The system is based on electrospun Polyamide 6,6 (PA 6,6) nonwovens soaked with a green solvent (dimethyl carbonate, DMC). The working principle of the system differs from previously tested gels and combined materials. The nonwoven, saturated with the cleaning agent, plays dual roles simultaneously. It functions as a retentive medium for the solvent that slowly infiltrates the varnish, causing its swelling, and acts as an adsorbent toward the swelled layer to be removed. Consequently, the aged coating can be easily peeled off from the substrate, avoiding the mechanical stresses usually required by other cleaning methods [8,14]. Furthermore, this cleaning system is user-friendly, its production can be scaled up, and the shape and size of the nonwoven can be adjusted to the specific need.

To investigate and elucidate the cleaning mechanism of the proposed system, we produced and tested electrospun nonwovens with varying thicknesses, fiber diameters, and pore dimensions. The nonwovens were impregnated with DMC, an alkyl carbonate that represents a green alternative to ketones and acetate esters. Indeed, DMC is biodegradable, has low environmental persistence, and presents minimal risk of bioaccumulation [25]. In addition, its volatility (boiling point 90.4 °C at atmospheric pressure) ensures that it does not persist within the paint layer [13,26–29]. The nonwovens were tested on mock-ups coated with a triterpene varnish (dammar), prepared following traditional recipes [30]. The assessment of cleaning efficiency, considering factors such as fiber residues and varnish removal, was carried out through micro-FTIR spectroscopy (Fourier Transformed InfraRed) in ATR (Attenuated Total Reflectance) mode and macro (MA) imaging (visible and UV-induced photoluminescence (PL)) [31–33]. An innovative analytical setup based on the integrated use of SEM (Scanning Electron Microscopy) and photoluminescence multispectral macro imaging (PL-MSMI) [34–36], was employed to assess the cleaning mechanism for the first time. Finally, initial exploratory tests were conducted on a 20th-century painting exhibiting an aged dammar coating.

2. Materials and methods

2.1. Materials

Dimethyl Carbonate (DMC, ReagentPlus®, 99 %) and 1,1,1,3,3,3-hexafluoro-2-propanol (HFIP, purity ≥ 99 %) were purchased from Sigma Aldrich. Polyamide 6,6 (PA 6,6, Zytel® E53 NC010) was kindly provided by DuPont. All chemical reagents are commercially available and were used as supplied without further treatment.

2.2. Electrospun nonwoven fabrication

A laboratory electrospinning machine (Spinbow Lab Unit, Spinbow S.r.1., Bologna, Italy) was used to fabricate PA 6,6 nonwoven tissues. The polymeric solution was dispensed from a syringe connected to a stainless-steel blunt-ended needle (inner diameter: 0.51 mm) through a PTFE tube, and an aluminum plate (10 cm × 10 cm) was used as a collector. PA 6,6 was dissolved in HFIP at room temperature (RT) under stirring overnight, at different concentrations, namely 10, 20, and 27 % w/V. Each solution was electrospun by applying the processing conditions reported in Table 1. Thus, three types of nonwovens were obtained, which differ in fiber diameter and pore dimension. Samples were labelled PA_0.4, PA_1, and PA_2, where the number indicates the

average fiber diameter of the corresponding mat expressed in micrometers. Different volumes of solutions were electrospun on the collector to obtain nonwovens with different thicknesses (in the range 150–650 μm) and grammages (gsm, in the range 15–105 g m^{-2}).

2.3. Paint mock-up preparation

The tests were carried out on a paint mock-up with layers prepared according to traditional recipes [30] and naturally aged over two years. A preparation layer of gypsum and rabbit glue (1.0 g of animal glue in 5.0 mL of hot distilled water mixed with 6.0 g of ground gypsum) was applied to the wooden support. The painting layer was obtained by dissolving 2.0 g of red-burnt ochre in 2.0 mL of 10 % w/w of rabbit glue solution. Finally, a triterpenoid varnish layer (1.0 g of dammar in 2.5 mL of turpentine) was applied [30]. The thickness of the varnish layer was monitored by observing painting cross-sections under an optical microscope using visible and UV light (Olympus Optical Microscope BX51, Tokyo, Japan).

2.4. Cleaning procedure

For each cleaning test, specimens of 0.7 cm × 0.7 cm were cut from the electrospun nonwoven, the specimens were then weighed, and their thickness was measured with a digital micrometer (Digimatic Micrometer, Mitutoyo Corporation). The ratio between the starting weight of each electrospun nonwoven and the volume of DMC to be added was established by progressively adding the solvent to a test mat (0.7 cm × 0.7 cm, known weight and thickness) until saturation. The following DMC volume/mat weight ratios were obtained and kept constant in all cleaning tests: 9 μL mg^{-1}, 7 μL mg^{-1}, and 5 μL mg^{-1} for PA_0.4, PA_1, and PA_2, respectively. In a typical test, the wet mat was gently positioned over the surface to be cleaned. After 5 min, the nonwoven was removed and no further mechanical action was employed to remove the dammar layer from the substrate.

2.5. Characterization of the nonwovens

Scanning electron microscope (SEM, Leica Cambridge Stereoscan 360) was performed at 20 kV accelerating on gold-sputtered samples. The distribution of fiber diameters was determined by Image J measuring about 200 fibers (trimming 2 % top–bottom, a subdivision in classes of 0.025 μm), and the results are given as the average diameter ± standard deviation of the mean (SD). The Student's *t*-test was used to verify the statistical significance of the difference between the mean values ($p < 0.05$).

The pore size distributions of the electrospun membranes were measured by capillary flow porometry (Porolux 1000, POROMETER, Belgium) by driving air through a wetted membrane to displace a pore-filling liquid (Galpore, fluid tension: 15.6 dyn cm^{-1}). The gas pressure gradually increases, and the liquid in the pores is progressively displaced as the pressure overcomes the capillary pressure of the pore, starting with the widest pores. The working temperature was 21° C, and the maximum pressure reached was 7 bar for PA_0.4 and 3 bar for PA_1 and PA_2. The mean pore size and pore size distribution were thus calculated. Three specimens (81.7 mm^2) were measured for each sample and averaged.

Solvent evaporation from the mats was monitored using gravimetric analysis and high-resolution PTR-TOF (Proton Transfer Reaction- Time-of-Flight). The former was carried out using an analytical balance. Samples with comparable thickness (PA_2 thickness: 500 μm, and PA_04 thickness: 400 μm) were weighted dry and set as tare. The proper amount of solvent, as described in Section 2.4, was quickly added to the sample, and the solvent evaporation was monitored by measuring the weight change every 10 s until stabilization. A high-resolution PTR-TOF instrument (Vocus CI-TOF, TOFWERK AG, Thun, Switzerland) was used for the real-time headspace measurement of DMC released from the electrospun nonwovens. Samples with comparable thickness were cut from the electrospun nonwovens, adding the proper amount of solvent, as described in Section 2.4. For this experiment, samples of different dimensions were employed to use the same amount of solvent. After keeping the DMC-soaked samples at RT for 5 min, they were placed on a 3 cm × 3 cm aluminum plate closed by a 3D-printed chamber (2.7 cm × 2.7 cm base, 3 cm height, Prusa I3 MK3, Prusa Research, Czech Republic) made of polylactic acid and equipped with a FilaFlexible40 gasket on the edge of the base (Figure S1). During the acquisition (30 min), clean supply air was flushed at a flow rate of 100 mL min^{-1} into the chamber inlet through a 3 m-long polytetrafluoroethylene (PTFE) tubing (1.55 mm o.d., 0.8 mm i.d.). Meanwhile, the sample was drawn at 100 mL min^{-1} at room temperature into the reagent ion source through a 1 m-long PTFE tubing (1.55 mm o.d., 0.8 mm i.d.). The Focusing Ion-Molecule Reactor (FIMR) was operated at a pressure of 2.5 mbar and, a radio frequency (RF) amplitude of 280 V and frequency of 2.3 × 10^6 Hz. The Vocus front and back voltages were 600 V and 45 V, respectively. The temperature of the reactor was set at 100 °C. The TOF mass analyzer was operated at a mass resolving power of 12,000–13,000 m Δm^{-1}, a mass range of 3–400 m/Q, and an extraction frequency of 14.3 kHz. The overtime variation of DMC was monitored through the target ion $C_3H_7O_3^+$ (m/Q 91.0395), where the m/Q ratio refers to the charger ion (H+, mass of 1 Th). The PTR-TOF instrument was calibrated daily using a reference gas mixture (Apel Riemer Environmental Inc., Florida, US) containing 13 different compounds (i.e., acetone, isoprene, benzene, acetaldehyde, methanol, acetonitrile, acrylonitrile, methyl ethyl ketone, toluene, m-xylene, α-pinene, 1,2,4-trimethylbenzene, β-caryophyllene) at a concentration level of 1 ppmv, which was 50-fold diluted with high-purity zero air generated from the instrument. The sensitivity for DMC measurement by Vocus PTR-TOF was 10,000 cps $ppbv^{-1}$. The concentration of DMC (VOC = Volatile Organic Solvent) was then calculated as the recorded signal divided by the sensitivity, as shown by Equation (1):

$$[VOC] = \frac{S_{VOC}(cps)}{S_{obs}} \quad (1)$$

Data were recorded using the TofDaq software (version 1.99.1425; Tofwerk AG) and processed using Tofware (version 2.3.5; Tofwerk AG). Background measurements of the system and the dry electrospun nonwovens were performed before each experiment. The bake-out of the headspace sampler at 50 °C and the aluminium plate at 150 °C for 30 min was carried out to prevent any carryover effect between subsequent experiments.

Table 1
Electrospinning processing conditions: polymer concentration, solution flow rate, voltage difference, needle-to-collector distance, temperature, and relative humidity registered during production. The average fiber diameter (±SD) (d) (n = 200) and average pore size (±SD) (D) (n = 3) are reported.

Sample	Conc. [% w v^{-1}]	Flow rate [mL h^{-1}]	Distance [cm]	Voltage [kV]	T [°C]	RH [%]	d [μm]	D [μm]
PA_0.4	10	1.5	20	20.5	18	53	0.4 ± 0.1	0.43 ± 0.08
PA_1	20	0.9	22	19.0	18	54	1.1 ± 0.1	2.2 ± 0.2
PA_2	27	1.0	18	11.3	20	50	2.0 ± 0.2	5.1 ± 0.9

2.6. Characterization of the mock-up and evaluation of the cleaning efficacy

μATR-FTIR spectroscopy was performed with a Thermo Nicolet (Thermo Fisher Scientific, Waltham, MA, USA), iN10MX imaging microscope fitted with a mercury-cadmium-telluride detector cooled with liquid nitrogen. Measurements were performed using a slide-on ATR objective equipped with a conical germanium crystal in the range 4000–675 cm^{-1}, at a spectral resolution of 4 cm^{-1} with 64 scans and an optical aperture of 400 μm × 400 μm. The analysis was performed before cleaning to collect reference spectra of the materials and after cleaning to evaluate the presence of varnish residues. Six spectra were collected in each area.

Photoluminescence multispectral macro imaging (PL-MSMI) was performed with a low-noise 1-megapixel Si electron multiplying CCD (EM-CCD) camera (Hamamatsu OORCA LT + 4.0) sensitive in the 350–1100 nm range. The camera was fitted with a UV–VIS-IR 60 mm 1:4 Apo Macro lens (CoastalOptics), in front of which was positioned a filter wheel holding 8 interference band-pass filters (Semrock) to collect images in selected spectral ranges. Illumination was provided by 16 LEDs of wavelengths ranging from 365 up to 700 nm (CoolLED pE-4000), coupled to a liquid light-guide fiber equipped with an annular light-guide allowing homogeneous illumination of the region of interest. The cleaning efficacy was measured using the optimized parameters (λ_{ex}: 365 nm, LED intensity: 100 %, filter: 514–30 nm, integration time: 10 s). Live monitoring was carried out in the same configuration, with integration time halved to 5 s to reach 0.2 frames per second (fps). The resulting digital images were processed using ImageJ [37,38].

Visible light macro photographs were collected with a stereomicroscope (Leica M125; 1.0 × objective, 0.8 × magnification) coupled to a camera (Leica FLEXACAM C1).

2.7. Characterization of the case study and cleaning tests

A real painting of the 20th century, provided by the Courtauld Institute of London for research purposes, was used to validate the cleaning system (Figure S2). From the edge where the paint film was already partially lifted, a micro-sample was collected and embedded in KBr and then in resin [39]. The different layers were identified thanks to optical microscopy, and the varnish layer's thickness was measured. μATR-FTIR analysis was then conducted to characterize the varnish, binder(s) and pigment(s). Three exploratory cleaning tests were conducted with PA_1 having thickness in the range of 340–270 μm coupled with DMC for 2 min and 30 s. The time of application was reduced as the thickness of the case study's varnish was lower than that of the mock-up, thus requiring less time to be absorbed. The effectiveness of the treatment was first assessed visually (photograph in visible and under UV light). Then, FTIR in reflectance mode was used to analyze the area before and after the cleaning treatment. The collected spectra have been denoised with wavelet (symlet 6 at level 3), and standard normalized deviation (SNV) was applied to correct the baseline.

3. Results and discussion

3.1. Characterization of the electrospun nonwovens

Nonwovens composed of randomly oriented fibers of PA 6,6 were fabricated by applying optimized electrospinning conditions (Table 1). In all instances, continuous, smooth, and bead-free fibers were obtained (Fig. 1a–c), and nonwovens were flexible and resistant to handling and folding. Leveraging the well-established correlation between polymer solution concentration and fiber diameter [40,41], we achieved varied fiber dimensions by simply adjusting the solution concentration while the other electrospinning conditions were set to ensure a stable and continuous jet during the process. The nonwovens display fiber diameters spanning both submicrometric and micrometric ranges, with an approximate 100 % diameter increase going from PA_0.4 to PA_1 and from PA_1 to PA_2 (see diameter distribution in Fig. 1d and average values in Table 1). It was previously reported that a linear correlation exists between fiber diameter and mean pore size [42]. Accordingly, in our nonwovens the variation in fiber diameter significantly influenced pore size, as evidenced by the concurrent increase in pore dimensions (Table 1 and Fig. 1). The resulting nonwovens showed an average fiber diameter and pore size of 0.45 μm / 0.43 μm, 0.98 μm / 2.2 μm and 2.2 μm / 5.1 μm, corresponding to the lowest, intermediate and highest polymer concentrations, respectively (Table 1), enabling the testing of

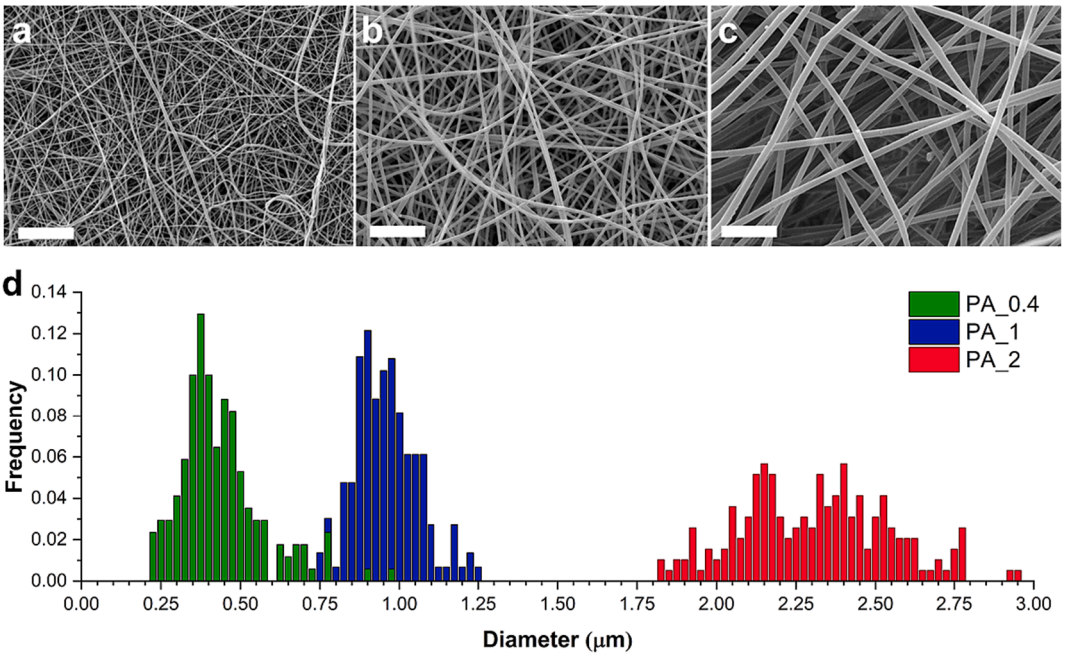

Fig. 1. Representative SEM micrographs of the electrospun nonwovens: (a) PA_0.4, (b) PA_1, (c) PA_2. Scale bar = 20 μm. (d) Fiber diameter distribution of PA_0.4 (green), PA_1 (blue), and PA_2 (red) (n = 200).

nonwovens with pore dimensions ranging from the submicrometric to the micrometric scale.

Liquid evaporation from porous materials can be delineated into three distinct steps [43,44]. In the initial step, the evaporation rate remains constant and has the maximum attainable value. This rate is determined by the liquid's saturated vapor pressure and the ambient temperature. The solvent evaporates from the pores of the material, generating a capillary flow from the wet internal regions towards the surface. The drying front progressively advances into the porous material until a specific critical depth is reached. The second step is characterized by a gradual reduction in the evaporation rate: the liquid evaporates from the smaller and deeper pores that are less accessible to the capillary flow. During the third stage, the evaporation rate stabilizes at a minimal value determined by the molecular diffusion of vapor through the dry zone. The liquid remains confined to the smallest, isolated pores, achieving equilibrium with the surrounding vapor. Therefore, according to these previous works [43,44], pore size should only influence the last stage of the evaporation process.

The influence of the nonwoven structure on DMC evaporation was investigated using two methodologies: (i) gravimetric analysis, conducted within the initial 5 min after DMC addition, to investigate the first stage of the evaporation process; (ii) PTR-TOF analysis, conducted starting from 5 min after DMC deposition, until complete solvent evaporation, to investigate the last stage of the process.

The first approach consists of recording the weight of the nonwoven soaked in DMC while the solvent is free to evaporate, and it was carried out on mats with comparable thickness and with the widest range of pore sizes (i.e. PA_04 and PA_2). Gravimetric measurements showed that after solvent addition, the evaporation rate of DMC is not affected by the different micro-to-nano porosities of the nonwovens since the solvent loss over time was essentially identical for the two tested materials (PA_04 wt variation over time: −0.086 mg s^{-1}, PA_2 wt variation over time: −0.088 mg s^{-1}; Fig. 2a).

PTR-TOF was carried out on electrospun samples of comparable thicknesses. The dimension of the samples was appropriately chosen to load the samples with the same absolute amount of solvent while maintaining the solvent/weight ratios indicated in Section 2.4. This expediency made it possible to exclude effects related to differing degrees of saturation within the chamber. Fig. 2b displays the concentration of DMC at various time points using PTR-TOF recorded after 5 min from solvent addition. Notably, it is more insightful to compare the behavioral trends of different materials rather than focusing on the absolute concentration values. By observing the trend of normalized concentration, a faster decrease in solvent concentration becomes apparent as the mat pore size decreases. This phenomenon can be attributed to the augmented surface area resulting from reduced porosity and fiber diameter, which contributes to the deceleration of DMC loss.

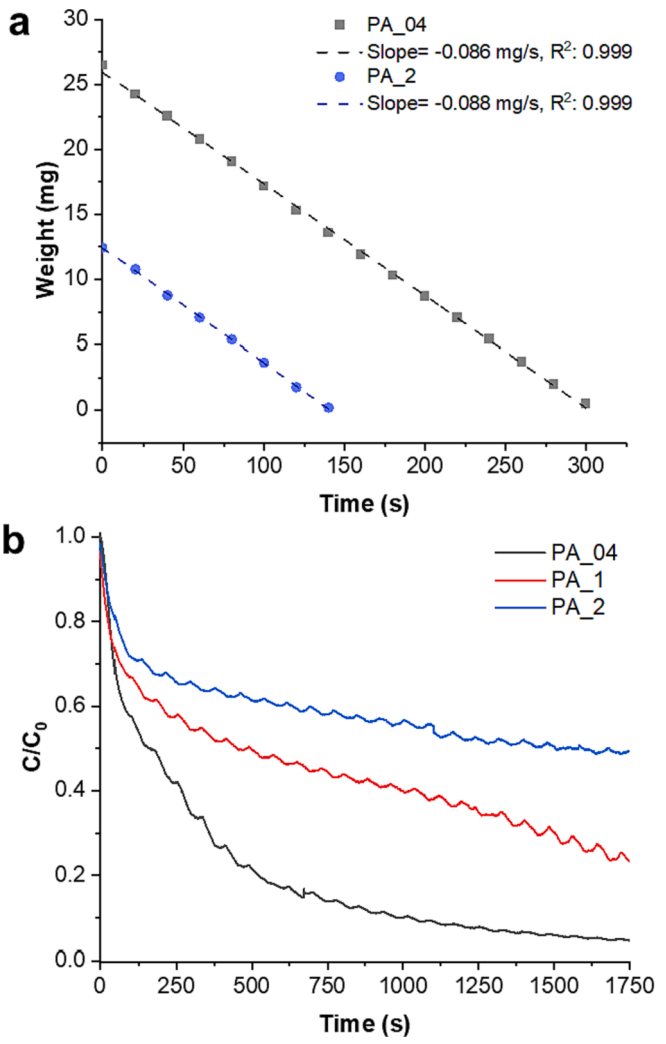

Fig. 2. Evaluation of solvent evaporation from the electrospun nonwovens. (a) Results of the gravimetric analysis reporting the weight of PA_04 (black) and PA_2 (blue) soaked in DMC as a function of time, with linear fitting (dashed lines), slope, and R^2. (b) PTR-TOF measurements: normalized concentration of DMC over time for PA_0.4 (black), PA_1 (red) and PA_2 (blue).

3.2. Assessment of the cleaning efficiency

Paint standard mock-ups were prepared to test the cleaning efficiency of the proposed ES nonwovens. Optical microscopy and μATR-FTIR spectroscopy were applied to characterize the cleaning mock-up areas before the cleaning procedure. The average varnish thickness, determined through microphotographs of sample cross-sections (Figure S3b and c), ranged from 40 to55 μm, consistent with the typical varnish thickness encountered in historical painting (10–60 μm) [45]. FTIR spectra were acquired from both the varnished and unvarnished surfaces of the mock-up (Figure S3a). In the paint layer spectra, we used characteristic spectral features to identify the glue binder (1635 cm^{-1} Amide I, 1533 cm^{-1} Amide II, 1450 cm^{-1} $\delta(CH_3)$/ $\delta(CH_2)$, 1411 cm^{-1} $\delta(CH_3)$ or $\nu(C{=}O) + \delta s(CH_3)$) [46–49] and the red ochre pigment (Si-O stretching at 1020 cm^{-1}) [50,51]. The dammar varnish can be identified by the antisymmetric and symmetric CH stretching (2931 cm^{-1} and 2869 cm^{-1}), the carbonyl stretching (1703 cm^{-1}), the CH bending (1454 cm^{-1} and 1383 cm^{-1}), the C—O/CC stretching at 1045 cm^{-1} and the out of plane CH bending at 889 cm^{-1} [52–56].

The electrospun nonwovens soaked in DMC were employed to remove the dammar coating from the mock-ups, with a contact time of 5 min and peeling off without applying any mechanical action, as described in Section 2.4. The comprehensive cleaning effectiveness was assessed through a multi-analytical approach utilizing PL-MSMI and μFTIR-ATR spectroscopy. Specifically, regions exhibiting discernible residues in the PL-MSMI images along with clear indications of dammar presence in the FTIR spectra were deemed incompletely cleaned.

As an example, Fig. 3 reports optical images, PL images, and μFTIR-ATR data of cleaning experiments carried out by using three different nonwovens with comparable thickness (Table 2: PA_0.4 entry 6; PA_1 entry 4; PA_2 entry 1). Images of the cleaned area clearly highlight that after cleaning with PA_0.4 and PA_1, the removal of dammar was effective (Fig. 3a–d). Conversely, the cleaning efficacy was unsatisfactory using the tissue with the largest fiber diameters and pores (PA_2) (Fig. 3e and f). In particular, the exceptional sensitivity of PL-MSMI enabled the assessment of varnish residues with excellent reliability and spatial accuracy. Indeed, by capturing the photophysical response of dammar, which appeared significantly more contrasted after optimization of the excitation and emission conditions [57,58], it became feasible to detect the presence of tiny patches of residue that would

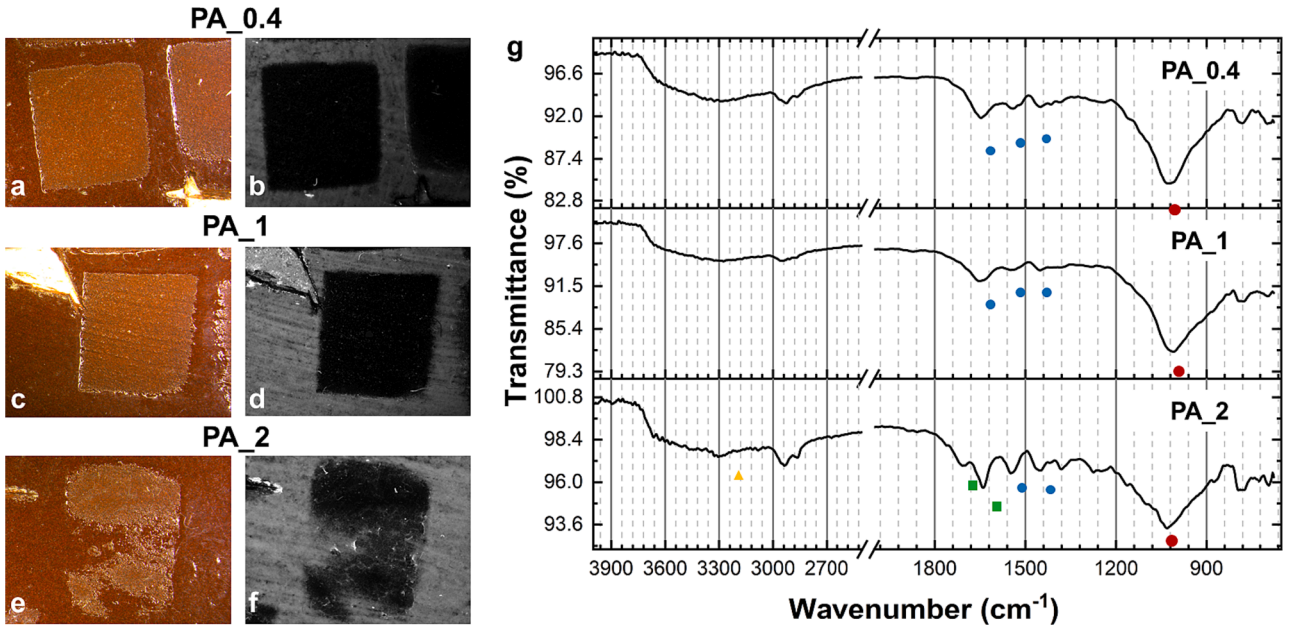

Fig. 3. Representative analyses for the determination of cleaning efficacy. a-c) Photographs were acquired with the stereomicroscope in visible light (a, c, and e). Images obtained with PL-MSMI (λ_{ex} = 365 nm, 514–30 nm filter, integration time = 10 s) (b, d and f). From top to bottom: tests performed with PA_0.4, PA_1, and PA_2. μFTIR-ATR spectra with identification of the characteristic peaks: glue (blue dot), red ochre (red dot), dammar (green square). From top to bottom: areas treated with PA_0.4, PA_1, and PA_2 (n = 6).

Table 2
List of the cleaning tests performed with the three PA 6,6 nonwovens with the variables considered (thickness, gsm, and volume of DMC added). For each test, the result of the cleaning efficiency assessed by the multi-analytical protocol is reported (see text for experimental details).

Sample	Entry	Thickness [μm]	gsm [g m^{-2}]	V[a] [μL]	Result
PA_0.4	1	134	15.31	6.75	Cleaned
	2	169	16.33	7.00	Cleaned
	3	190	18.57	16.00	Cleaned
	4	227	20.00	9.00	Cleaned
	5	271	24.29	10.00	Cleaned
	6	386	42.90	19.00	Cleaned
	8	398	49.80	20.00	Cleaned
	9	461	53.67	24.00	Cleaned
PA_1	1	151	20.41	7.00	Incomplete cleaning
	2	208	28.57	10.00	Cleaned
	3	245	41.43	14.00	Cleaned
	4	335	40.82	14.00	Cleaned
	5	361	46.94	16.00	Cleaned
	6	373	53.06	18.00	Cleaned
	7	376	46.94	17.00	Cleaned
	8	400	63.27	21.00	Cleaned
	9	405	57.14	20.00	Cleaned
	10	408	59.18	21.00	Cleaned
	11	426	58.37	20.00	Cleaned
	12	443	55.10	19.00	Cleaned
	13	526	61.22	21.00	Cleaned
PA_2	1	393	65.31	16.00	Incomplete cleaning
	2	394	67.35	17.00	Incomplete cleaning
	3	402	65.31	16.00	Incomplete cleaning
	4	447	71.43	17.00	Incomplete cleaning
	5	458	62.86	22.00	Incomplete cleaning
	6	535	75.51	18.00	Incomplete cleaning
	7	565	93.88	32.00	Incomplete cleaning
	8	592	83.67	28.00	Incomplete cleaning
	9	638	104.90	26.00	Incomplete cleaning
	11	666	100.61	25.00	Incomplete cleaning

[a] The following DMC volume/mat weight ratios were kept constant in all cleaning tests: 9 μL mg^{-1}, 7 μL mg^{-1}, and 5 μL mg^{-1} for PA_0.4, PA_1, and PA_2, respectively.

otherwise remain undetectable through other imaging techniques. μATR-FTIR analyses confirmed the results of the PL-MSMI, detecting the presence of dammar residues when the treatment was not fully effective (Fig. 3g). Indeed, the areas cleaned with PA_0.4 and PA_1 show the characteristic bands of the glue binder (1635 cm^{-1}, 1533 cm^{-1}, 1450 cm^{-1}) and the red ochre pigment (1000 cm^{-1}) in the paint layer. Differently, the area treated with PA_2 displays characteristic peaks of dammar (1703 cm^{-1}, 1455 cm^{-1}, 1374 cm^{-1}), highlighting the poor cleaning efficacy. Furthermore, fiber residues were observed with optical microscopy.

Each material was tested, its thickness and grammar (gsm) varying (Table 2). Considering all the cleaning tests reported in Table 2, we observed that the best results in terms of cleaning efficacy were obtained by using PA_0.4 and PA_1, while nonwovens made by fibres with the largest diameter and the widest pores, i.e. PA_2, showed the poorest cleaning performance. The DMC volumes range from a minimum of 7 μL to a maximum of 32 μL, depending on sample thickness. No evident cleaning role played by the amount of solvent is detectable. As an example, comparing experiments performed by keeping constant the used volume (Table 2: PA_0.4 entry 3; PA_1 entry 5; PA_2 entry 1), it turns out that the cleaning efficacy is different and only depends on nonwoven structure (i.e., fiber and pore diameter).

It is worth mentioning that the peel-off effect exploited by the tissues allowed the operator to avoid the additional use of cotton swabs, usually necessary to remove the swollen varnish present on the surface after the treatment. This one-step procedure represents a significant advantage in terms of non-invasiveness toward the object and a novelty compared to the most widespread chemical cleaning systems.

To better highlight the outcomes of the experiments, Fig. 4 plots each experiment which is identified by the the thickness and gsm of the employed nonwoven. Additionally, each test has been color-coded (green and red), with red representing an incomplete cleaning (i.e., varnish residues remaining after cleaning), and green representing a successful cleaning. As expected, there is a linear correlation between the mat thickness and the grammage (Fig. 4 a–c). All cleaning experiments were successful for PA_0.4 nonwoven, tested with gsm in the 15–55 g m^{-2} range. In the case of PA_1, tested in the range 20–65 g m^{-2}, cleaning experiments were almost entirely satisfactory. Unsuccessful

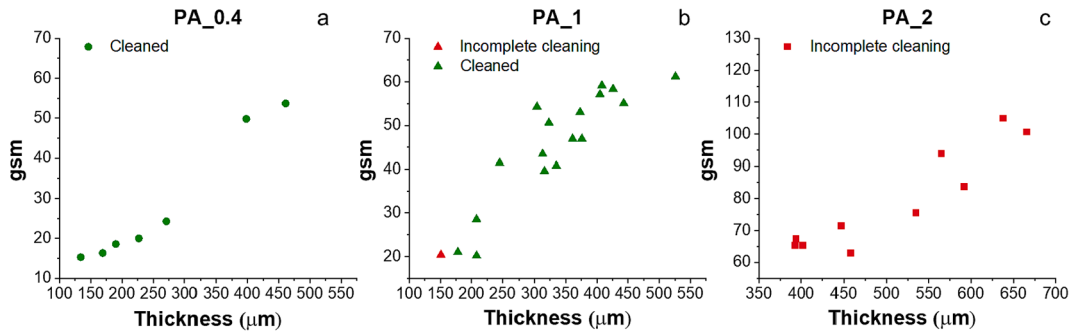

Fig. 4. Graphical representation of the cleaning tests, reporting gsm as a function of nonwoven thickness: a) PA_0.4, b) PA_1, and c) PA_2. The red color was assigned to tests with a negative outcome, while the green one was given to positive tests.

results were instead obtained using PA_2 samples in all ranges of grammage tested (60–100 g m^{-2}). It is worth mentioning that for these last samples, preliminary tests using nonwovens with lower values of gsm were carried out (not showed) that, similarly, were not adequate for cleaning.

3.3. Cleaning mechanism

Based on the obtained results, the cleaning efficacy appears to depend solely on the microporosity of the mats. This hypothesis was confirmed by SEM observations of the nonwoven section with medium pore size (Table 2, PA_1, entry 4) after cleaning (Fig. 5a–d). High magnifications of the bottom side in contact with the painting surface (green), middle part (blue), and upper side (red) are reported. The dammar residues, highlighted in pink (original SEM analyses are reported in Figure S4), were identified based on their distinct morphological characteristics. Specifically, a comparison of SEM images of the mats before and after cleaning reveals the presence of round-shaped particles entrapped within the fiber network, which were absent in the original nonwoven material. It can be noted that the pores of the nonwovens, located near the side in contact with the painting surface, exhibit a dense accumulation of varnish residues. The amount of these residues gradually decreases towards the central and uppermost regions of the material.

Interestingly, dammar is found to be distributed throughout the entire thickness of the sample rather than being confined solely to the layer in contact with the paint. This observation suggests that the fibers do not act only as a gripping site for the swelled varnish. Notably, this behavior was also observed in PA_0.4 nonwovens. For comparison, Fig. 5e–g reports the SEM cross-section of the nonwoven with large pore size and comparable thickness (Table 2, PA_2 entry 1, original SEM images are reported in Figure S5).

Similarly to PA_1, dammar residues can be observed within the material; however, their quantity appears smaller, in line with the previously noted inferior cleaning efficiency. These qualitative observations can be reasonably motivated by the different capillary rises in nonwovens having different pore sizes: the smaller the pore dimension, the greater the height to which the dammar detached from the mock-up rises within the porosities of the nonwoven. Consequently, the amount of varnish that the nonwoven can remove depends on its porosity.

To gain further insights into the cleaning mechanism, the PL-MA imaging setup was tentatively employed to live-monitor the cleaning process, exploiting the fluorescence of dammar. Correlating the PL variation with the evolution of a process is commonly used in the biomedical field to monitor living cells, physiological dynamics, or drug release [59,60]. In the field of cultural heritage, this technique has occasionally been used to assess the final effectiveness of conservation treatment. However, to our knowledge, this is the first time it has been

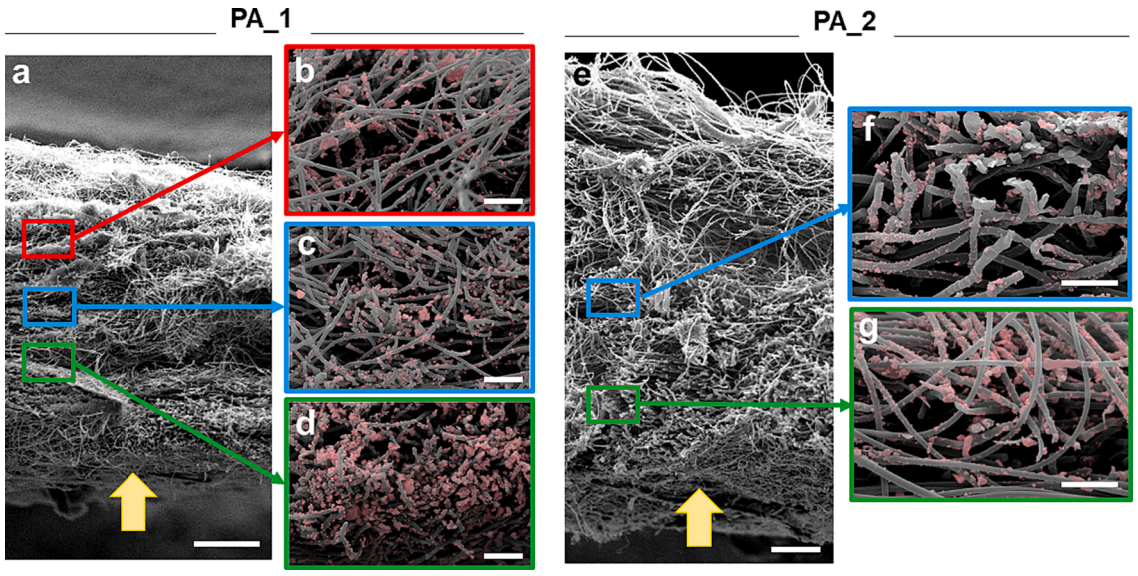

Fig. 5. A) SEM micrograph of pa_1 section after cleaning (entry 4 inTable 2). Closer inspections of the upper side of the sample, not in contact with the paint (b, red), the middle area of the sample (c, blue), and the bottom side, in contact with the paint (d, green). e) SEM micrograph of PA_2 section after cleaning (entry 1 in Table 2). Closer inspections of the upper side of the sample middle area (f, blue) and the bottom side, in contact with the paint (g, green). The dammar residues are marked in pink color. The yellow arrow points to the side of the sample in contact with the paint mock-up. Scale bars: 100 μm (a and e); 20 μm (b-d, f and g).

used to monitor a cleaning treatment.

The experiment was carried out using the different nonwovens with comparable thickness soaked in DMC and placed on the varnished mock-up. PL images were collected every 5 s during the cleaning procedure for up to 5 min. A control experiment was carried out by monitoring the PL of a representative nonwoven (PA_0.4) soaked with DMC and placed on a glass slide, without dammar, to assess whether the solvent evaporation could affect the nonwoven PL. For each timelapse consisting 60 frames, three frames are reported in Fig. 6a–d. All the nonwovens applied to the varnished mock-up (Fig. 6a–c) showed a progressive increase in PL signal over time, whereas the PL remained relatively stable for the sample applied to the glass slide (Fig. 6d). The increase in PL intensity

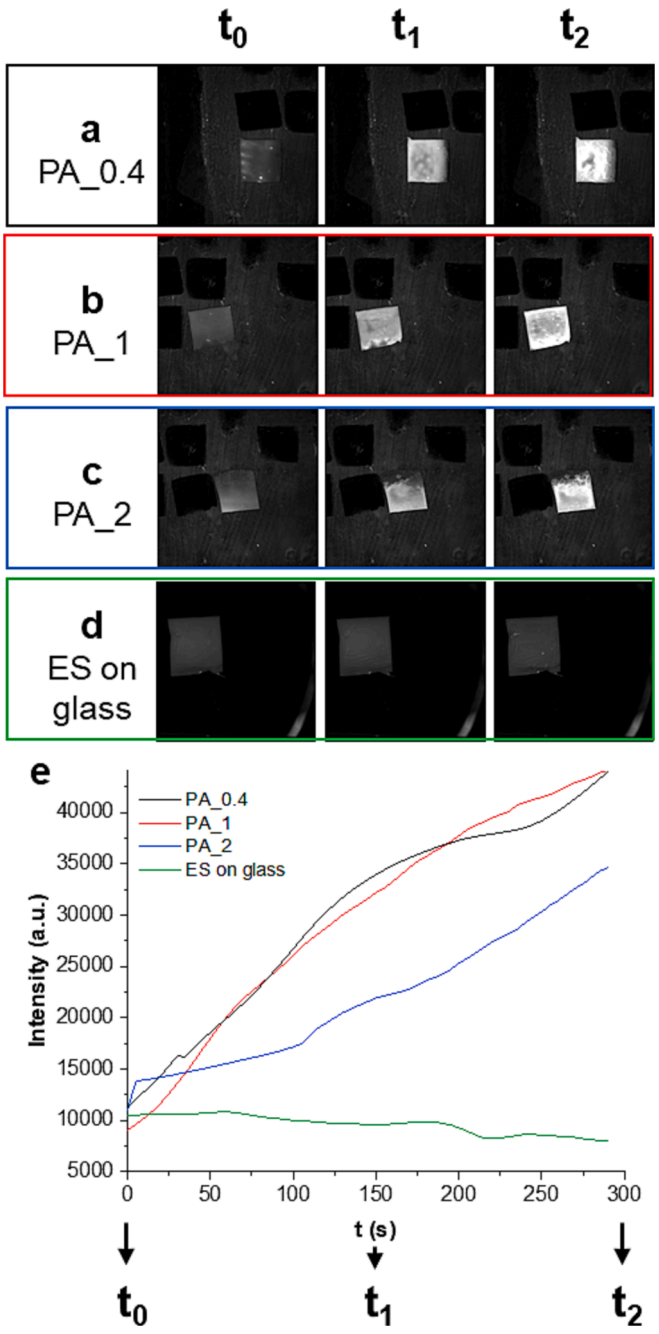

Fig. 6. Live monitoring of the cleaning process with PL-MA imaging. Images at t0 (0 s), t1 (150 s), and t2 (299 s) of PA_0.4 (a), PA_1 (b), PA_2 (c), and PA_0.4 on a glass slide (d). e) Pixel intensity over time determined from the time-lapses recorded for PA_0.4 (black), PA_1 (red), PA_2 (blue), and PA_0.4 on the glass slide (green).

following the cleaning process can be attributed to the gradual infiltration of dammar into the pores of the nonwovens, whose emission is highly scattered within the mat porosity.

We quantified the PL variations for all the nonwovens by extracting the z-plot (pixel intensity vs. time) in the nonwoven area using Image J (Fig. 6e). The pixel intensity was adjusted by subtracting the background value (either the varnish layer or the glass slide) in each frame. The photoluminescence of the electrospun nonwoven soaked in DMC did not change over time when placed on a glass slide (green curve in Fig. 6e), confirming that the solvent evaporation did not affect the PL intensity. On the contrary, when the mats were applied to the varnished mock-up, the PL gradually increased over time (red, blue, and black curves in Fig. 6e). The PL rise of PA_2 is slower (blue curve, slope: 74.85 a.u. s^{-1}) and reaches a lower value at the end of the experiment compared to both PA_0.4 (black curve, slope: 108.3 a.u/s) and PA_1 (red curve, slope: 121.7 a.u. s^{-1}). This outcome indirectly confirms that PA_0.4 and PA_1 showed a similar cleaning behaviour, while PA_2 had a lower varnish uptake, thus a worse cleaning efficiency.

Based on all our results, Fig. 7 reports a scheme to describe the cleaning mechanism. Initially, when the nonwoven saturated with DMC comes into contact with the varnish, the primary driving force for the swelled dammar to diffuse into the mat is the solvent evaporation occurring at the upper surface of the nonwoven whose rate, according to the experimental data presented in Section 3.1, appears constant and quite similar for the three mats, as can be observed by comparing the slopes in the weight versus time plots reported in (Fig. 2a).

Consequently, the varnish concentration within the mat increases at the surface in contact with the paint mock-up. This establishes a varnish concentration gradient between the lower part of the mat and its external surface, which acts as an additional driving force for the diffusion of the coating material into the mat porosities. As the solvent continues to evaporate, the capillary rise draws the dissolved varnish further into the mat. In essence, the mechanism of cleaning and varnish peeling-off can be ascribed to three concomitant phenomena: 1) the evaporation of the cleaning agent, 2) the capillary rise of the swelled varnished in the mat pores, and 3) the diffusion process of the varnish driven by the concentration gradient (Fig. 7). The pore dimension solely affects the second phenomenon. Indeed, as reported in Section 3.1, the evaporation rate in the first minutes is unaffected by the pore size of the mats. At the same time, it is well-established that the lower the pore dimension, the higher the capillary rise [61]. Thus, the efficient peeling-off mechanism observed using low and medium-pore-size nonwovens can reasonably be ascribed to the increase of capillary rise resulting from small pore size.

Interestingly, previous research on the use of DMC as a cleaning agent showed that satisfactory results could not be obtained when it was applied using cotton swabs due to its high volatility [13]. We demonstrated that using a gel as a carrier of DMC reduced the solvent evaporation and increased its contact time with the varnish, resulting in an effective swelling of the varnish that, however, required mechanical action for its complete removal [13]. In the present study, the cleaning process was further improved and simplified by using electrospun nonwovens, in which the combination of evaporation rate and capillary rise allowed for coating removal without mechanical actions. This shows that solvents that have been progressively abandoned due to their inefficiency with current carriers could potentially be reinstated using novel carriers with significantly different physisorption/evaporation properties.

3.4. Validation on a case study

Optical microscopy and μATR-FTIR spectroscopy were applied to characterize the stratigraphy composition of the case study (Figure S2). Fig. S6a shows that the painting stratigraphy presented a preparatory layer, a paint layer and a varnish layer. The average varnish thickness, evaluated through microphotographs of sample cross-sections, was

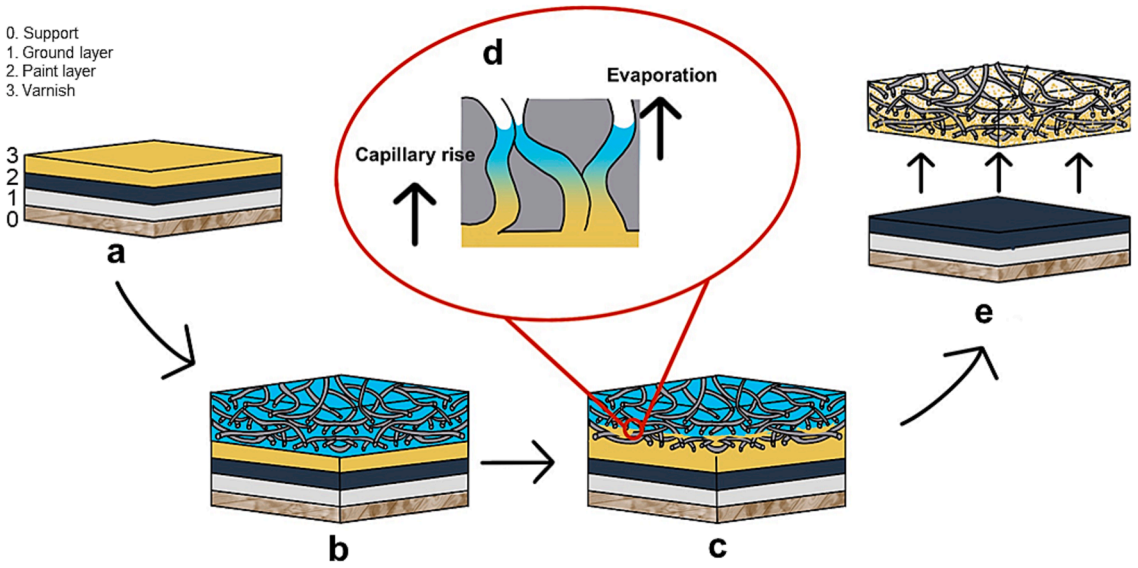

Fig. 7. Schematic representation of the cleaning procedure: a) cross-section of the painting; b) application of an electrospun nonwoven soaked with solvent over the painting in contact with the varnish; c) swelling of the varnish and adsorption within the mat with a close-up of the proposed mechanism (d); e) peel-off of the mat and cleaned area.

20–30 μm. In the paint layer FTIR spectrum (Fig. S6b), we used characteristic spectral features to identify the oil binder (2920 cm^{-1} and 2950 cm^{-1} antisymmetric and symmetric CH stretching, 1737 cm^{-1} carbonyl stretching) [62] and lead white pigment (3535 cm^{-1}, 1399 cm^{-1}) [63,64]. The presence of Lead carboxylates was also identified by the diagnostic peak at 1517 cm^{-1} [64]. The dammar varnish can be identified by the antisymmetric and symmetric CH stretching (2925 cm^{-1} and 2860 cm^{-1}), the carbonyl stretching (1712 cm^{-1}), and the CH bending (1457 cm^{-1} and 1380 cm^{-1}) [52–56]. In the preparation layer, oil, lead white and calcium carbonate (872 cm^{-1}) were identified [50].

As all the cleaning tests performed on the case study yielded similar results, we present a representative example (PA_1, thickness = 350 μm, 21 μL of DMC, time of application = 2′ 30′′). As illustrated in Fig. 9, even on aged and deteriorated paint, the proposed system allowed paint removal through a peel-off effect without additional mechanical action with cotton swabs. This is achieved as the swelled varnish is entirely absorbed into the electrospun mat. It is important to note that, in contrast to the mock-up prepared in the laboratory, the paint surface of the case study exhibits noticeable unevenness. Consequently, paint residues remain in the depressions corresponding to the brush strokes. These observations are further confirmed by FTIR analysis in reflection, where a decrease in the bending of the derivative of the typical dammar peaks is observed (1701 cm^{-1} carbonyl stretching and CH bending 1450 cm^{-1}). These preliminary tests indicate the applicability of the developed cleaning system to authentic cases.

4. Conclusions

This work introduces a novel cleaning system based on electrospun PA 6,6 nonwovens saturated with a green solvent, DMC, where the nonwoven acts as both a retentive medium for controlled solvent release and an adsorbent for the swelled varnish. The peel-off effect observed in the proposed system eliminates the need for additional mechanical action, making it a user-friendly and non-invasive alternative to traditional cleaning methods. Cleaning efficiency was tested on mock-ups coated with dammar varnish using three different PA mats with increasing fiber and pore diameters: PA_0.4 (fiber diameter = 0.45 μm; pore diameter = 0.43 μm), PA_1 (fiber diameter = 0.98 μm; pore diameter = 2.2 μm), and PA_2 (fiber diameter = 2.2 μm; pore diameter = 5.1 μm). The nonwovens with smaller pore sizes exhibit superior performance, with PA_0.4 and PA_1 achieving satisfactory results, while PA_2 shows lower

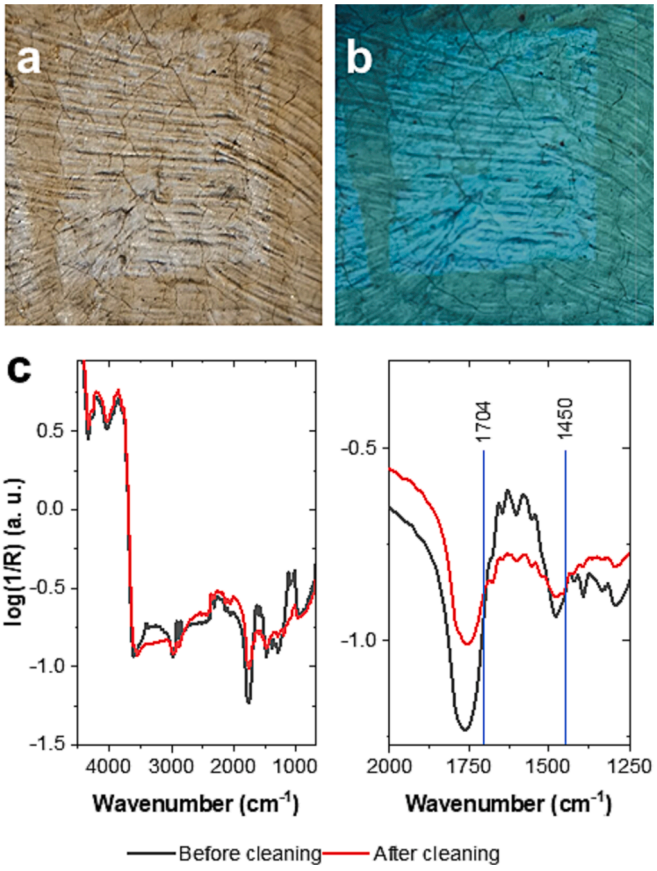

Fig. 9. Photographic documentation of the cleaning tests performed using PA_1 nonwoven on the case study "Sea landscape" under (a) visible light and (b) UV light. c) Reflectance spectra collected on the same area before (black) and after (red) cleaning. The entire spectral range is on the left, and the region 2000–1250 cm^{-1} is on the right with the identification of dammar characteristic peaks. SNV baseline correction was applied on both spectra.

cleaning efficacy. Advanced analytical techniques, including micro-FTIR spectroscopy, PL-MSMI, and SEM, were employed to characterize the mat, elucidate the cleaning mechanism, and evaluate the system's efficacy. The live monitoring of the cleaning process using PL imaging represents a novel contribution to the field. The multi-analytical approach allows to identify three fundamental phenomena that contribute to the successful cleaning: the evaporation of the cleaning agent, the capillary rise of the swelled varnished in the mat pores, and the diffusion process of the varnish driven by the concentration gradient. While the pore size does not influence the solvent evaporation during the time of the cleaning action, the capillary rise increases as the pore size of the mats decreases. These combined effects contribute to the dissolution and diffusion of the varnish. Solvent evaporation establishes a concentration gradient, while capillary rise helps to draw dissolved varnish deeper into the electrospun tissues, especially when the tissues have small pore sizes. The proposed cleaning system's applicability is further demonstrated in a case study with an authentic painting exhibiting aged paint coating. The developed electrospun nonwoven-based cleaning system offers a promising alternative to existing methods, such as the application of organic solvents with cotton swabs or gels, which suffer from limitations such as poor solvent confinement, volatility, and toxicity [5]. The system provides improved control over solvent release, scalability, and adaptability to various restoration needs. This research contributes to ongoing efforts in the restoration field, aligning with principles of non-invasiveness towards cultural heritage objects and ensuring operator safety. Future research will explore the application of these methods in other industrial fields where selective, effective, and controlled removal of unwanted substances is necessary. Additionally, the development of new formulations using biobased or recycled polymers for electrospun materials will enable the proposal of more environmentally sustainable solutions.

CRediT authorship contribution statement

Francesca Ramacciotti: Writing – original draft, Visualization, Validation, Investigation, Formal analysis. **Giorgia Sciutto:** Writing – review & editing, Supervision, Conceptualization. **Laure Cazals:** Writing – original draft, Investigation, Formal analysis. **Denise Biagini:** Writing – original draft, Methodology, Investigation, Formal analysis. **Serena Reale:** Writing – original draft, Investigation, Formal analysis. **Ilaria Degano:** Writing – review & editing, Supervision, Resources, Methodology. **Maria Letizia Focarete:** Conceptualization, Supervision, Writing – review & editing, Resources. **Rocco Mazzeo:** Supervision, Resources. **Mathieu Thoury:** Writing – review & editing, Supervision, Resources, Methodology. **Loïc Bertrand:** Writing – review & editing, Supervision, Resources, Methodology. **Chiara Gualandi:** Writing – review & editing, Supervision, Resources, Conceptualization. **Silvia Prati:** Writing – review & editing, Supervision, Methodology, Funding acquisition, Conceptualization.

Declaration of competing interest

The authors declare the following financial interests/personal relationships which may be considered as potential competing interests: [Chiara Gualandi, Francesca Ramacciotti, Giorgia Sciutto, Maria Letizia Focarete, Rocco Mazzeo, Silvia Prati has patent issued to WO2023006859A1. If there are other authors, they declare that they have no known competing financial interests or personal relationships that could have appeared to influence the work reported in this paper].

Data availability

Data will be made available on request.

Acknowledgement

This research has been funded by the Horizon Europe project GoGreen, "Green strategies to conserve the past and preserve the future of cultural heritage" (G.A. no. 101060768). We thank SAATI SPA for their support in the porometric analysis. LB and LC acknowledge support from the DIM PAMIR of the Île-de-France Region in the ENS Imaging equipment project context. We thank the Center for Instrument Sharing of the University of Pisa (CISUP) for allowing us to use the PTR-TOF. We acknowledge Tobias Burderer and Francesca Modugno for the fruitful discussion of the PTR-TOF results. Finally, this research was part of an ongoing study carried out in the frame of the PRIN2020 project "SUPERSTAR - Sustainable Preservation Strategies for Street Art" (2022-2025), an Italian network project (https://prin2020superstar.dcci.unipi.it/) funded by the Italian Ministry of University. We thank the Courtauld Institute of London, particularly Dr Austin Nevin and Clare Richardson, for allowing the new cleaning system on authentic artworks to be tested.

Appendix A. Supplementary data

Supplementary data to this article can be found online at https://doi.org/10.1016/j.jcis.2024.03.006.

References

[1] S. Prati, F. Volpi, R. Fontana, P. Galletti, L. Giorgini, R. Mazzeo, L. Mazzocchetti, C. Samorì, G. Sciutto, E. Tagliavini, Sustainability in art conservation: a novel bio-based organogel for the cleaning of water sensitive works of art, Pure Appl. Chem. 90 (2018) 239–251, https://doi.org/10.1515/pac-2017-0507.
[2] M. Matteini, R. Mazzeo, A. Moles, Chemistry for restoration: painting and restoration materials, Nardini Editore (2016).
[3] A. Phenix, J. Townsend, A brief survey of historical varnishes, Conserv. Easel Paint. (2020) 262–273, https://doi.org/10.4324/9780429399916-13.
[4] E. Kargioti, E. Vouvoudi, C. Nannou, D. Bikiaris, D. Lambropoulou, Unraveling the origin of aged varnishes for the proper restoration of old paintings using spectroscopic and spectrometric techniques, Microchem. J. 168 (2021), https://doi.org/10.1016/J.MICROC.2021.106467.
[5] A. Phenix, R.C. Wolbers, J. Townsend, S. Zumbühl, A. Bartoletti, J. Lee, B. Ormsby, Removal of varnish: organic solvents as cleaning agents, Conserv. Easel Paint. (2020) 549–573, https://doi.org/10.4324/9780429399916-37.
[6] L. Baij, J. Buijs, J.J. Hermans, L. Raven, P.D. Iedema, K. Keune, J. Sprakel, Quantifying solvent action in oil paint using portable laser speckle imaging, Sci. Rep. 10 (2020), https://doi.org/10.1038/S41598-020-67115-1.
[7] P. Cremonesi, Combination of a liquid-dispensing and micro-aspiration device for the cleaning of sensitive painted surfaces, Stud. Conserv. 63 (2018) 315–325, https://doi.org/10.1080/00393630.2017.1396029.
[8] C. Samorì, P. Galletti, L. Giorgini, R. Mazzeo, L. Mazzocchetti, S. Prati, G. Sciutto, F. Volpi, E. Tagliavini, The green attitude in art conservation: polyhydroxybutyrate–based gels for the cleaning of oil paintings, ChemistrySelect. 1 (2016) 4502–4508, https://doi.org/10.1002/slct.201601180.
[9] A. Macchia, L. Rivaroli, B. Gianfreda, The GREEN RESCUE: a 'green' experimentation to clean old varnishes on oil paintings, Nat. Prod. Res. 35 (2021) 2335–2345, https://doi.org/10.1080/14786419.2019.1675061.
[10] D. Stulik, D. Miller, H. Khanjian, R. Wolbers, J. Carlson, W.C. Peterson, Solvent gels for the cleaning of works of art: the residue question, The Getty Conservation Institute, 2004.
[11] C. Riedo, G. Rollo, O. Chiantore, D. Scalarone, Detection and identification of possible gel residues on the surface of paintings after cleaning treatments, Heritage. 4 (2021) 304–315, https://doi.org/10.3390/HERITAGE4010019.
[12] S. Khanna, A.K. Srivastava, Recent advances in microbial polyhydroxyalkanoates, Process Biochem. 40 (2005) 607–619, https://doi.org/10.1016/j.procbio.2004.01.053.
[13] S. Prati, G. Sciutto, F. Volpi, C. Rehorn, R. Vurro, B. Blümich, L. Mazzocchetti, L. Giorgini, C. Samorì, P. Galletti, E. Tagliavini, R. Mazzeo, Cleaning oil paintings: NMR relaxometry and SPME to evaluate the effects of green solvents and innovative green gels, New J. Chem. 43 (2019) 8229–8238, https://doi.org/10.1039/c9nj00186g.
[14] Y. Jia, G. Sciutto, R. Mazzeo, C. Samorì, M.L. Focarete, S. Prati, C. Gualandi, Organogel coupled with microstructured electrospun polymeric nonwovens for the effective cleaning of sensitive surfaces, ACS Appl. Mater. Interfaces. 12 (2020) 39620–39629, https://doi.org/10.1021/ACSAMI.0C09543.
[15] a) J. Xue, T. Wu, Y. Dai, Y. Xia, Electrospinning and electrospun nanofibers: Methods, materials, and applications, Chem. Rev. 119 (2019) 5298–5415. 10.1021/acs.chemrev.8b00593; b) A. Greiner, J. H. Wendorff, Electrospinning: A fascinating method for the preparation of ultrathin fibers, Angewandte Chemie - International Edition 46 (2007) 5670-5703. 10.1002/anie.200604646; c) D. H. Reneker, A. L. Yarin, Electrospinning jets and polymer nanofibers, Polymer 49 (2008) 2387-2425. 10.1016/j.polymer.2008.02.002.

[16] S. Chigome, N. Torto, A review of opportunities for electrospun nanofibers in analytical chemistry, Anal. Chim. Acta. 706 (2011) 25–36, https://doi.org/10.1016/J.ACA.2011.08.021.
[17] L. Persano, A. Camposeo, C. Tekmen, D. Pisignano, Industrial upscaling of electrospinning and applications of polymer nanofibers: a review, Macromol. Mater. Eng. 298 (2013) 504–520, https://doi.org/10.1002/MAME.201200290.
[18] D. Li, Y. Xia, Electrospinning of nanofibers: reinventing the wheel? Adv. Mater. 16 (2004) 1151–1170, https://doi.org/10.1002/ADMA.200400719.
[19] J.V. Patil, S.S. Mali, A.S. Kamble, C.K. Hong, J.H. Kim, P.S. Patil, Electrospinning: a versatile technique for making of 1D growth of nanostructured nanofibers and its applications: an experimental approach, Appl. Surf. Sci. 423 (2017) 641–674, https://doi.org/10.1016/j.apsusc.2017.06.116.
[20] D. Hussain, S.T. Raza Naqvi, M.N. Ashiq, M. Najam-ul-Haq, Analytical sample preparation by electrospun solid phase microextraction sorbents, Talanta. 208 (2020) 120413, https://doi.org/10.1016/J.TALANTA.2019.120413.
[21] J. Yuan, R. Gao, Y. Wang, W. Cao, Y. Yun, B. Dong, J. Dou, A novel hydrophobic adsorbent of electrospun SiO2@MUF/PAN nanofibrous membrane and its adsorption behaviour for oil and organic solvents, J. Mater. Sci. 53 (2018) 16357–16370, https://doi.org/10.1007/S10853-018-2795-1.
[22] Y. Yu, Q. Ma, J. bin Zhang, G. bin Liu, Electrospun SiO2 aerogel/polyacrylonitrile composited nanofibers with enhanced adsorption performance of volatile organic compounds, Appl. Surf. Sci. 512 (2020) 145697, https://doi.org/10.1016/J.APSUSC.2020.145697.
[23] Y.S. Ryu, S.H. Kim, Research of polylactide porous hollow nanofiber membrane with high selective absorption characteristics, J. Appl. Polym. Sci. 137 (2020) 49132, https://doi.org/10.1002/APP.49132.
[24] M. Amorini, N. Riboni, L. Pesenti, V.A. Dini, A. Pedrini, C. Massera, C. Gualandi, F. Bianchi, R. Pinalli, E. Dalcanale, Reusable cavitand-based electrospun membranes for the removal of polycyclic aromatic hydrocarbons from water, Small. 18 (2022), https://doi.org/10.1002/smll.202104946.
[25] C. Samorì, M. Basaglia, S. Casella, L. Favaro, P. Galletti, L. Giorgini, D. Marchi, L. Mazzocchetti, C. Torri, E. Tagliavini, Dimethyl carbonate and switchable anionic surfactants: two effective tools for the extraction of polyhydroxyalkanoates from microbial biomass, Green Chem. 17 (2015) 1047–1056, https://doi.org/10.1039/C4GC01821D.
[26] P. Ferrari, D. Chelazzi, N. Bonelli, A. Mirabile, R. Giorgi, P. Baglioni, Alkyl carbonate solvents confined in poly (ethyl methacrylate) organogels for the removal of pressure sensitive tapes (PSTs) from contemporary drawings, J. Cult. Herit. 34 (2018) 227–236, https://doi.org/10.1016/J.CULHER.2018.05.009.
[27] D. Delledonne, F. Rivetti, U. Romano, Developments in the production and application of dimethylcarbonate, Appl. Catal. Gen. 221 (2001) 241–251, https://doi.org/10.1016/S0926-860X(01)00796-7.
[28] D. Seo, Toxicity assessment of dimethyl carbonate following 28 days repeated inhalation exposure, Environ. Anal. Health Toxicol. 36 (2021), https://doi.org/10.5620/EAHT.2021012.
[29] J. Yiming, G. Sciutto, S. Prati, E. Catelli, M. Galeotti, S. Porcinai, L. Mazzocchetti, C. Samorì, P. Galletti, L. Giorgini, E. Tagliavini, R. Mazzeo, A new bio-based organogel for the removal of wax coating from indoor bronze surfaces, Herit. Sci. 7 (2019) 1–12, https://doi.org/10.1186/s40494-019-0276-8.
[30] C. Cennini, Il libro dell'arte, I Colibrì (2003).
[31] E.A. Willneff, S.L.M. Schroeder, B.A. Ormsby, Spectroscopic techniques and the conservation of artists' acrylic emulsion paints, Herit. Sci. 2 (2014) 1–10, https://doi.org/10.1186/S40494-014-0025-Y/FIGURES/7.
[32] S. Prati, G. Sciutto, I. Bonacini, R. Mazzeo, New Frontiers in application of FTIR microscopy for characterization of cultural heritage materials, Top. Curr. Chem. 374 (2016), https://doi.org/10.1007/S41061-016-0025-3.
[33] J.P. Echard, M. Thoury, B.H. Berrie, T. Séverin-Fabiani, A. Vichi, M. Didier, M. Réfrégiers, L. Bertrand, Synchrotron DUV luminescence micro-imaging to identify and map historical organic coatings on wood, Analyst. 140 (2015) 5344–5353, https://doi.org/10.1039/C5AN00483G.
[34] M. Picollo, M. Stols-Witlox, L.F. López, UV-Vis Luminescence: Imaging Techniques, Editorial Universitat Politècnica de València, 2019. https://monografias.editorial.upv.es/index.php/con_360/article/view/94 (accessed January 24, 2023).
[35] Broad-Band, Photo-Induced, Steady-State Luminescence Imaging in Practice, in: UV-Vis Lumin. Imaging Tech., Editorial Universitat Politècnica de València, 2019: pp. 61–102. https://monografias.editorial.upv.es/index.php/con_360/article/view/94 (accessed January 24, 2023).
[36] M. Thoury, M. Elias, J.M. Frigerio, C. Barthou, Nondestructive varnish identification by ultraviolet fluorescence spectroscopy, Appl. Spectrosc. 61 (2007) 1275–1282, https://doi.org/10.1366/000370207783292064.
[37] C.A. Schneider, W.S. Rasband, K.W. Eliceiri, NIH image to ImageJ: 25 years of image analysis, Nat. Methods. 9 (2012) 671–675, https://doi.org/10.1038/NMETH.2089.
[38] J. Schindelin, I. Arganda-Carreras, E. Frise, V. Kaynig, M. Longair, T. Pietzsch, S. Preibisch, C. Rueden, S. Saalfeld, B. Schmid, J.-Y. Tinevez, D.J. White, V. Hartenstein, K. Eliceiri, P. Tomancak, A. Cardona, Fiji: an open-source platform for biological-image analysis, Nat. Methods. 9 (2012) 676–682, https://doi.org/10.1038/nmeth.2019.
[39] S. Prati, F. Rosi, G. Sciutto, P. Oliveri, E. Catelli, C. Miliani, R. Mazzeo, Evaluation of the effect of different paint cross section preparation methods on the performances of fourier transformed infrared microscopy in total reflection mode, Microchem. J. 110 (2013) 314–319, https://doi.org/10.1016/j.microc.2013.04.016.
[40] P. Gupta, C. Elkins, T.E. Long, G.L. Wilkes, Electrospinning of linear homopolymers of poly(methyl methacrylate): exploring relationships between fiber formation, viscosity, molecular weight and concentration in a good solvent, Polym. U. K. 46 (2005) 4799–4810, https://doi.org/10.1016/j.polymer.2005.04.021.
[41] S.L. Shenoy, W.D. Bates, H.L. Frisch, G.E. Wnek, Role of chain entanglements on fiber formation during electrospinning of polymer solutions: good solvent, non-specific polymer–polymer interaction limit, Polymer. 46 (2005) 3372–3384, https://doi.org/10.1016/j.polymer.2005.03.011.
[42] H. Ma, C. Burger, B.S. Hsiao, B. Chu, Ultra-fine cellulose nanofibers: new nano-scale materials for water purification, J. Mater. Chem. 21 (2011) 7507–7510, https://doi.org/10.1039/C0JM04308G.
[43] M. Gonçalves, J.Y. Kim, Y. Kim, N. Rubab, N. Jung, T. Asai, S. Hong, B.M. Weon, Droplet evaporation on porous fabric materials, Sci. Rep. 12 (2022) 1087, https://doi.org/10.1038/s41598-022-04877-w.
[44] N. Shokri, M. Prat, P. Coussot, Editorial: saline water evaporation from porous media, Transp. Porous Media. 128 (2019) 857–859, https://doi.org/10.1007/s11242-019-01290-2.
[45] O. Kokkinaki, E. Dimitroulakos, K. Melessanaki, D. Anglos, P. Pouli, O. Kokkinaki, E. Dimitroulakos, K. Melessanaki, D. Anglos, P. Pouli, Laser-induced fluorescence as a non-invasive tool to monitor laser-assisted thinning of aged varnish layers on paintings: fundamental issues and critical thresholds, EPJP. 136 (2021) 938, https://doi.org/10.1140/EPJP/S13360-021-01929-4.
[46] H. Fabian, W. Mäntele, Infrared spectroscopy of proteins, Handb. Vib. Spectrosc. (2006), https://doi.org/10.1002/0470027320.S8201.
[47] K. Belbachir, R. Noreen, G. Gouspillou, C. Petibois, Collagen types analysis and differentiation by FTIR spectroscopy, Anal. Bioanal. Chem. 395 (2009) 829–837, https://doi.org/10.1007/S00216-009-3019-Y.
[48] A. Barth, Infrared spectroscopy of proteins, Biochim. Biophys. Acta BBA - Bioenerg. 1767 (2007) 1073–1101, https://doi.org/10.1016/J.BBABIO.2007.06.004.
[49] S. Olsztyńska-Janus, A. Pietruszka, Z. Kiełbowicz, M.A. Czarnecki, ATR-IR study of skin components: lipids, proteins and water. part I: temperature effect, Spectrochim. Acta. a. Mol. Biomol. Spectrosc. 188 (2018) 37–49, https://doi.org/10.1016/J.SAA.2017.07.001.
[50] F.A. Miller, C.H. Wilkins, Infrared spectra and characteristic frequencies of inorganic ions, Anal. Chem. 24 (2002) 1253–1294, https://doi.org/10.1021/AC60068A007.
[51] R.A. Nyquist, R.O. Kagel, Infrared spectra of inorganic compounds (3800-45cm^{-1}), (1997) 140.
[52] C.-M. Popescu, C. Vasile, B.C. Simionescu, Gheorghe spectral characterization of natural resins used in conservation, Rev Roum Chim. 57 (2012) 495–499.
[53] C. Azémard, C. Vieillescazes, M. Ménager, Effect of photodegradation on the identification of natural varnishes by FT-IR spectroscopy, Microchem. J. 112 (2014) 137–149, https://doi.org/10.1016/J.MICROC.2013.09.020.
[54] M.H. Franz, I. Neda, C.V. Maftei, I. Ciuca, D. Bolcu, M.M. Stănescu, Studies of chemical and mechanical properties of hybrid composites based on natural resin dammar formulated by epoxy resin, Polym. Bull. 78 (2021) 2427–2438, https://doi.org/10.1007/S00289-020-03221-4.
[55] I. Bonaduce, F. Di Girolamo, I. Corsi, I. Degano, M.R. Tinè, M.P. Colombini, Terpenoid oligomers of dammar resin, J. Nat. Prod. 79 (2016) 845–856, https://doi.org/10.1021/ACS.JNATPROD.5B00916.
[56] D. Ciofini, J. Striova, M. Camaiti, S. Siano, Photo-oxidative kinetics of solvent and oil-based terpenoid varnishes, Polym. Degrad. Stab. 123 (2016) 47–61, https://doi.org/10.1016/J.POLYMDEGRADSTAB.2015.11.002.
[57] A. Nevin, J.-P. Echard, M. Thoury, D. Comelli, G. Valentini, R. Cubeddu, Excitation emission and time-resolved fluorescence spectroscopy of selected varnishes used in historical musical instruments, Talanta. 80 (2009) 286–293, https://doi.org/10.1016/j.talanta.2009.06.063.
[58] M. Thoury, J.-P. Echard, M. Réfrégiers, B. Berrie, A. Nevin, F. Jamme, L. Bertrand, Synchrotron UV-visible multispectral luminescence microimaging of historical samples, Anal. Chem. 83 (2011) 1737–1745, https://doi.org/10.1021/ac102986h.
[59] A. Ettinger, T. Wittmann, Fluorescence live cell imaging, Methods Cell Biol. 123 (2014) 77, https://doi.org/10.1016/B978-0-12-420138-5.00005-7.
[60] Z. Fan, L. Sun, Y. Huang, Y. Wang, M. Zhang, Bioinspired fluorescent dipeptide nanoparticles for targeted cancer cell imaging and real-time monitoring of drug release, Nat. Nanotechnol. 11 (2016) 388–394, https://doi.org/10.1038/nnano.2015.312.
[61] J. Berthier, Theory of wetting, micro-drops digit, Microfluid. (2013) 7–73, https://doi.org/10.1016/B978-1-4557-2550-2.00002-X.
[62] R. Mazzeo, E. Joseph, S. Prati, A. Millemaggi, Attenuated Total reflection-fourier transform infrared microspectroscopic mapping for the characterization of paint cross-sections, Anal. Chim. Acta. 599 (2007) 107–117, https://doi.org/10.1016/j.aca.2007.07.076.
[63] E. Pięta, J. Olszewska-Świetlik, C. Paluszkiewicz, A. Zając, W.M. Kwiatek, Application of ATR-FTIR mapping to identification and distribution of pigments, binders and degradation products in a 17th century painting, Vib. Spectrosc. 103 (2019) 102928, https://doi.org/10.1016/j.vibspec.2019.102928.
[64] A.C. Blanco Guerrero, I.A. Millán, V.P. Careaga, G. Siracusano, M.S. Maier, A multi-analytical approach for the characterization of painting materials and metal soap formation in two artworks by the argentinian painter Antonio berni, Minerals. 13 (2023), https://doi.org/10.3390/min13070919.